Contribution from the Department of Chemistry,
The University of Chicago, Chicago, Illinois 60637

Aspects of Metal–Metal Bonding in Early-Transition-Metal Dioxides

JEREMY K. BURDETT* and TIMOTHY HUGHBANKS

Received October 1, 1984

A theoretical investigation of metal–metal-bonded clusters and extended networks within dioxide frameworks is presented. In particular, we examine metal–metal bonding and the influence exerted by the oxide "matrix" within hollandites, octahedral layers, and trigonal-prismatic layers. For d^2–$d^{2.5}$ hollandite systems, distortions of zigzag Mo chains are coupled to π interactions with trigonal-planar oxides that stitch the double chains of the structure together. Zigzag chains embedded within CdI_2-like layers are stable for electron counts at which one would expect discrete clusters within a hollandite framework. As in chalcogenides, trigonal-prismatic transition-metal dioxide layers are expected to be most stable for d^2 metals. The stability of the trigonal-prismatic layer compounds $LiNbO_2$ and $NaNbO_2$ is understandable as compared with octahedral alternatives and as compared with distorted variants of the trigonal-prismatic structure.

Introduction

Metal–metal-bonded systems in solids may adopt structures in which the metal–metal-bonded network is broken into separate islands of two or a few centers or extends infinitely in one, two, or three dimensions throughout the material in question. Recent synthetic work on binary, ternary, and quaternary transition-metal dioxides is supplementing our pool of examples in which nature's choice between localized and extended networks is yet to be understood. In this work we turn our attention to a few examples, mostly from molybdenum dioxide chemistry, in which the interplay between metal–metal bonding and the structures in which the metal–metal-bonded network is enclosed is particularly intriguing.

The majority of binary transition-metal oxides adopt the rutile structure **1** or a distorted variant in at least one of their polymorphic forms.[1] The rutile structure can be described as composed of single chains of edge-sharing octahedra (see **2**) that are

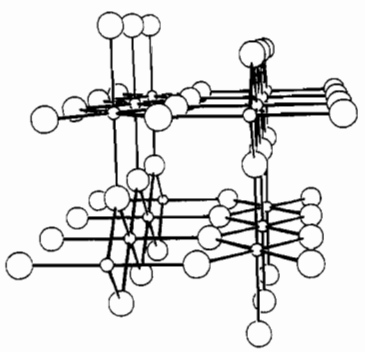

1

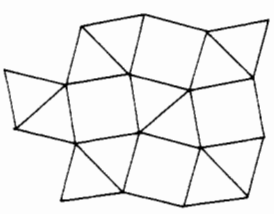

2

joined along their lengths by sharing corners. In **1** we show a projection along the length of the chains. Structures intermediate between rutile and that of octahedral layer compounds may be constructed by joining multiple octahedral chains in similar ways. Thus, the hollandite[2] (α-MnO_2) structure **3** and the ramsdellite structure **4** are built from double chains, as shown in **5**. Of course,

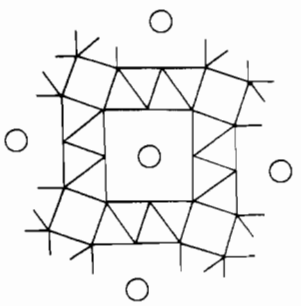

3

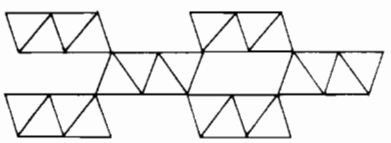

4

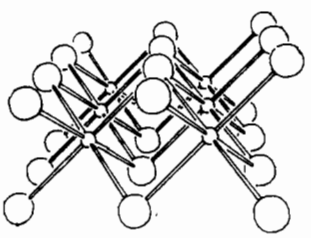

5

a MO_2 layer compound is obtained as the "multiplicity" of a "chain" goes to infinity and interchain linkages do not occur.

The structures adopted by a particular system appear to be crucially influenced by the presence or absence of cations that may reside in the channels or between the layers (see **6**) of a given

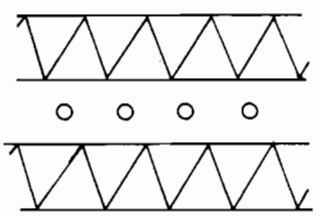

6

MO_2 network. For example, McCarley and co-workers[3] synthesized a compound with the stoichiometry $Ba_{1.14}Mo_8O_{16}$, which adopts a distorted hollandite (**3**) structure, and another specimen with the composition $Na_{0.85}Mo_2O_4$,[4] which adopts a CdI_2-like (**6**)

(1) Wells, A. F. "Structural Inorganic Chemistry", 5th ed.; Oxford University Press: Oxford, England, 1984.
(2) (a) Byström, A.; Byström, A. M. *Acta Crystallogr.* **1950**, *3*, 146. (b) Recent structural refinements of hollandites and related phases may be found in: Post, J. E.; Von Dreele, R. B.; Buseck, P. B. *Acta Crystallogr., Sect. B: Struct. Crystallogr. Cryst. Chem.* **1982**, *B38*, 1056.
(3) Torardi, C. D.; McCarley, R. E. *J. Solid State Chem.* **1981**, *37*, 393.
(4) McCarley, R. E.; Lii, K.-H.; Edwards, P. A.; Brough, L. F. *J. Solid State Chem.*, in press. The Na^+ ion stoichiometry is somewhat uncertain in this compound.

0020-1669/85/1324-1741$01.50/0

layer structure (again, distorted) in which the Na^+ ions partially occupy the interstices between octahedral layers. (This structure is then like $NaFeO_2$.)[1] These compounds are in contrast to MoO_2 itself, which adopts a distorted rutile structure with Mo atoms forming dimers somewhat twisted away from the chain axis. We suspect that, other factors being equal (if that is possible), the choice of structure type is largely a result of the "size" requirements of the counterions in question. For example, the rutile structure contains distorted octahedral interstices but they are far too small to accommodate Ba^{2+} or even Na^+. On the other hand, insertion compounds (Li_xMO_2: $x = 1$, M = Mo; $0.2 < x < 0.9$, M = Ru, Ir) have been prepared in which Li^+ inhabits these interstices.[6-9] These compounds can be viewed as NiAs-type derivatives as well, and indeed the oxide arrangement in the rutile host is known to move quite close to a hcp arrangement. The formerly trigonal-planar oxides of the rutile structure become pyramidal to accommodate the incoming Li^+ ions as illustrated in **7**. (Our usual,

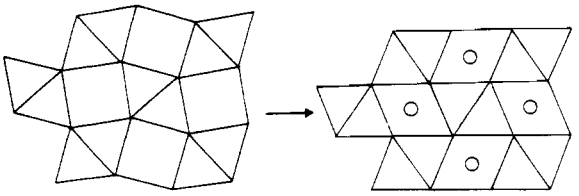

7

often implicit, assumptions about the "innocence" of the Li^+ counterions may be suspect given that Ru–Li distances of 2.53 Å are found in $Li_{0.87}RuO_2$, as would be expected on viewing the structure as a NiAs derivative.)

The main focus of the present work will be on the ways in which the transition-metal atoms (usually Mo) arrange themselves within the frameworks in which they are encapsulated.[5] Specifically, we wish to understand the reasons underlying the distortions alluded to above in the compounds $Na_{0.85}Mo_2O_4$ and $Ba_{1.14}Mo_8O_{16}$. In the former material the Mo atoms move off the positions they would occupy in an ideal hexagonal net expected for an undistorted octahedral layer. As shown in **8**, zigzag double chains are formed

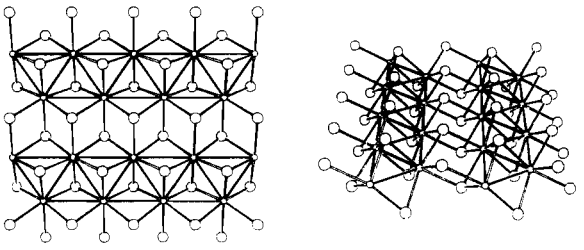

8

with short Mo–Mo bonds between strings and moderate distances are found within strings (2.53 and 2.89 Å, respectively). This arrangement of metal–metal bonds suggests a description of the structure in which the layers are seen as being built from edge-sharing octahedral double chains. Such a description allows more direct comparison with the material $Ba_{1.14}Mo_8O_{16}$. If we take the octahedral double chain found in $Na_{0.85}Mo_2O_4$ as a building block, it is not difficult to imagine a metal–metal-bonded hollandite analogue assembled by corner sharing of the chains, as illustrated in **9**. In $Ba_{1.14}Mo_8O_{16}$ this is what happens except Mo atoms within the double chains distort from the zigzag arrangement depicted in **8** to form clusters as indicated in **10**. The situation

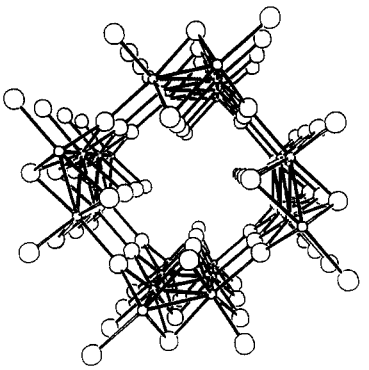

9

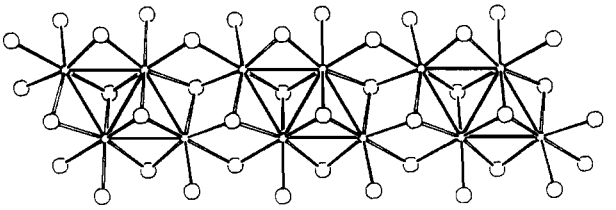

10

is further complicated by the existence of two different kinds of chains: in the first type the clusters are nearly regular rhombuses with Mo–Mo distances all close to 2.59 Å; in the second type the clusters are distorted so that two nonadjacent outer Mo–Mo distances are lengthened to about 2.85 Å while the three other bonds are approximately 2.55 Å long. Torardi and Calabrese have recently made a similar compound with the composition $K_2Mo_8O_{16}$ in which all the principal features of this pseudohollandite compound are found as well, including both distorted and undistorted Mo_4 clusters.[10]

In very recent work, Torardi has synthesized $BaRu_6O_{12}$ in which one finds a RuO_2 network that adopts a hollandite structure as in **9** in which Ru–Ru contacts average 3.05 Å and are all longer than 2.9 Å.[11] No marked distortion indicative of Ru clustering is evident. Ba^{2+} ions occupy 67% of available sites in the channels of the structure, yielding the observed stoichiometry.

Why does the layered $Na_{0.85}Mo_2O_4$ distort from a hexagonal structure to form the zigzag ribbons seen in **8**? Even more puzzling, why in the hollandite analogue $Ba_{1.14}Mo_8O_{16}$ are the potentially reasonable zigzag chains further distorted to form clusters and, given that there is indeed clustering, why are there two different kinds? Is metal–metal bonding significant in $BaRu_6O_{12}$, and if it is not, how does this compound utilize its incompletely filled Ru d orbitals (the Ru atoms are formally $d^{4.33}$)? In what follows, we present results and observations that exhibit our qualitative and still incomplete understanding of the answers to these questions.

Qualitative Features of MO Layers

Let us first examine the electronic structure of an ideal (undistorted) MoO_2 layer. First, we make the customary division of the metal d orbitals into pseudo-e_g and -t_{2g} sets in accordance with whether or not they are directed for σ or π overlap with the octahedron of surrounding oxide ligands. The t_{2g} orbitals are left free to form metal–metal bonds within the layer and are also potentially available for Mo–O π interaction. It turns out that the bands of importance for describing Mo–Mo bonding can be fairly adequately understood by using a quite simple approach.

We will consider each Mo atom to reside at the origin of a local coordinate system such that the threefold axis of rotation that is normal to the plane of the MoO_2 layer goes through the Mo center and lies on the line given by the equation $x = y = z$. Then the "t_{2g}" orbitals of each metal are labeled in the usual way: i.e., as xy, xz, and yz (see **11**). Given this, let us consider a simple model

(5) (a) Metal–metal bonding in molecular alkoxides is discussed in: Chisholm, M. H.; Huffman, J. C.; Kirkpatrick, C. C.; Leonelli, J. *J. Am. Chem. Soc.* **1981**, *103*, 6093. See also: (b) Chisholm, M. H.; Folting, K.; Huffman, J. C.; Kirkpatrick, C. C. *Inorg. Chem.* **1984**, *23*, 1021 and references therein.
(6) Murphy, D. W.; DiSalvo, F. J.; Carides, J. N.; Waszczak, J. V. *Mater. Res. Bull.* **1978**, *13*, 1395.
(7) Cox, D. E.; Cava, R. J.; McWhan, D. B.; Murphy, D. W. *J. Phys. Chem. Solids* **1982**, *43*, 657.
(8) Schöllhorn, R. *Angew. Chem.* **1980**, *92*, 1015; *Angew. Chem., Int. Ed. Engl.* **1980**, *19*, 983.
(9) Davidson, I. J.; Greedan, J. E. *J. Solid State Chem.* **1984**, *51*, 104.
(10) Torardi, C. C.; Calabrese, J. C. *Inorg. Chem.* **1984**, *23*, 3281.
(11) Torardi, C. C. *Mater. Res. Bull.*, in press.

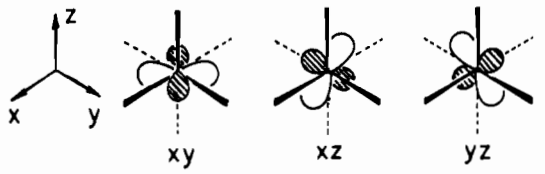

11

for describing metal–metal bonding within the layer: each t_{2g} d orbital will be considered to interact only with orbitals on neighboring metals with the same label. That is, we allow only *xy–xy*, *xz–xz*, and *yz–yz* interactions. When we so restrict the possible d–d nearest-neighbor interactions, the band structure of the t_{2g} subblock is entirely determined by the translational symmetry (Bloch's theorem) and a few reasonance integrals (β_σ, β_π, and β_δ) between interacting d orbitals. In **12** we show the res-

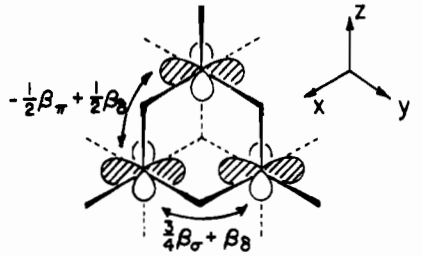

12

onance integrals of interest. The resonance integrals shown follow directly from the angular-overlap decomposition of the indicated interactions. Interactions are shown between *xy* orbitals on adjacent metals; the threefold axis through the metal makes it obvious that *xz–xz* and *yz–yz* interactions will be identical.

Since we have not allowed any mixing between our basis d orbitals and have ignored the effect of Mo d–O p π interaction, we can write the form of the wave functions for the "t_{2g}"-derived d bands directly from translational symmetry requirements (i.e. Bloch's theorem):

$$\psi_{xy}(\vec{k}) = \frac{1}{N^{1/2}}\sum_{\vec{R}} e^{i\vec{k}\cdot\vec{R}}\chi_{xy}(\vec{r} - \vec{R}) \qquad (1)$$

This expression merely indicates that the form of the energy band wave functions is determined by the wave vector $\vec{k}$, which in turn fixes the phase factor, $\exp(i\vec{k}\cdot\vec{R})$, between metal atom orbitals separated by a two-dimensional direct lattice vector $\vec{R}$. In **13** we

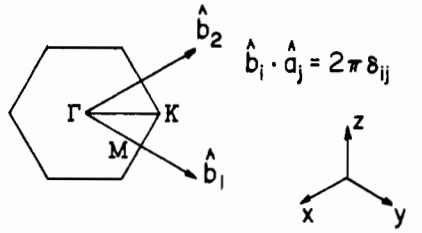

13

show the first Brillouin zone, constructed as described in standard texts,[12] which shows the region of $\vec{k}$ space to which we may restrict our attention. The form of the energy bands as a function of $\vec{k}$ (i.e., the dispersion) may be found by evaluating the energy of $\psi_{xy}(\vec{k})$ directly:

$$\epsilon_{xy}(\vec{k}) = \langle\psi_{xy}(\vec{k})|\mathcal{H}_{\text{eff}}|\psi_{xy}(\vec{k})\rangle = {}^3/_2\beta_\sigma \cos k_1 - \beta_\pi[\cos k_2 + \cos(k_1 + k_2)] + \beta_\delta[{}^1/_2 \cos k_1 + \cos k_2 + \cos(k_1 + k_2)] \qquad (2)$$

where we assume overlap can be neglected in the normalization and $\vec{k}$ is expressed as $\vec{k} = k_1\hat{b}_1 + k_2\hat{b}_2$. Expressions for $\epsilon_{xz}(\vec{k})$ and $\epsilon_{yz}(\vec{k})$ can be obtained by permuting the variables k_1, k_2, and $(k_1 + k_2)$ in eq 2: for $\epsilon_{xz}(\vec{k})$ change k_1 to $(k_1 + k_2)$, k_2 to k_1, and $(k_1 + k_2)$ to k_2; for $\epsilon_{yz}(\vec{k})$ change k_1 to k_2, k_2 to $(k_1 + k_2)$, and $(k_1 + k_2)$ to k_1.

(12) (a) Harrison, W. A. "Solid State Theory"; Dover: New York, 1980. (b) Ashcroft, N. W.; Mermin, N. D. "Solid State Physics"; Holt, Rinehart and Winston: New York, 1976. (c) Lax, M. "Symmetry Principles in Solid State and Molecular Physics"; Wiley: New York, 1974.

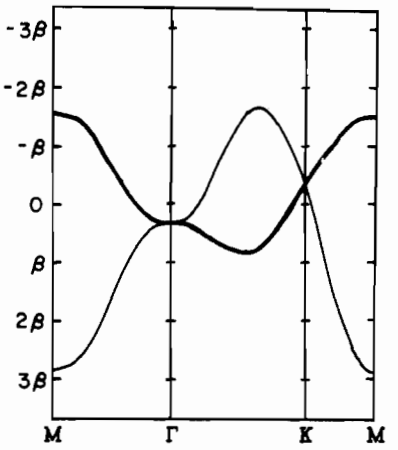

Figure 1. Energy bands from the simple Hückel model for metal–metal interactions in a hexagonal layer, plotted on the high-symmetry lines of the Brillouin zone. The heavy line is doubly degenerate.

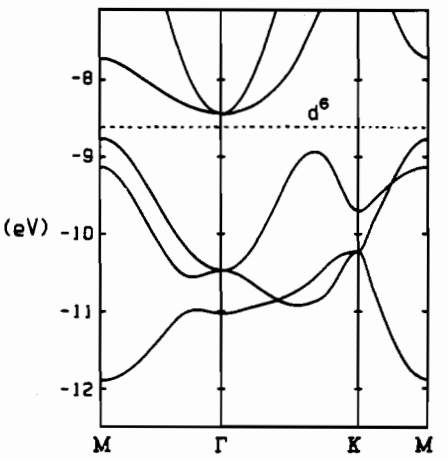

Figure 2. Calculated Mo d bands for a MoO_2 layer. Note the correspondence with the model bands displayed in Figure 1.

In order to finally construct our crude band structure from expressions for $\epsilon_{xy}(\vec{k})$, $\epsilon_{xz}(\vec{k})$, and $\epsilon_{yz}(\vec{k})$, we assume the resonance integrals β_σ, β_π, and β_δ will scale as the corresponding overlaps S_σ, S_π, and S_δ, as in the usual Wolfsberg–Helmholz approximation. Using values for these overlaps calculated for Mo atoms spaced 2.87 Å apart, we obtain $\beta_\delta = 0.153\beta$, $\beta_\pi = 0.783\beta$, and $\beta_\sigma \equiv \beta$ ($S_\delta = 0.0116$, $S_\pi = 0.0592$, $S_\sigma = 0.0756$). In Figure 1 we show a plot of our model band structure along high-symmetry lines in the Brillouin zone. Heavy lines indicate doubly degenerate levels for these symmetry lines.

How well does this rather crude model represent the results of a detailed calculation? In Figure 2 we show the Mo d bands that result from an extended Hückel (EH) calculation on the full MoO_2 layer (see the Appendix for details on this and subsequent calculations). The oxide p bands lie below the bottom of the energy range depicted, and the Mo "e_g" bands may be seen to lie wholly above the d^6 line indicated at about −8.6 eV. The three low-lying "t_{2g}" bands show an obvious resemblance to the simple model band structure derived above. Indeed, when the Wolfsberg–Helmholz approximation is used to obtain a value for β in Figure 1 ($\beta = 0.875H_{dd}S_\sigma = 0.73$ eV), the bandwidth of the model is quite close to that in the full calculation. Clearly, the overall form of the dispersion curves changes only modestly on moving from the idealized picture in Figure 1 to the more realistic bands of Figure 2.

Not surprisingly, the greatest differences between the two figures occur where degeneracies are found in the idealized picture. The treatment outlined above ignores any coupling between $\psi_{xy}(\vec{k})$,

$\psi_{xz}(\vec{k})$, and $\psi_{yz}(\vec{k})$. From perturbation theory it is expected that the splittings induced by introducing any coupling will be greatest when the interacting levels are degenerate. One source of this coupling is direct metal–metal interaction; that is, the basis functions $\psi_{xy}(\vec{k})$, $\psi_{xz}(\vec{k})$, and $\psi_{yz}(\vec{k})$ are not orthogonal. It is a straightforward matter to see that two out of the six xz orbitals adjacent to an xy orbital have a nonzero overlap, as illustrated in **14**. An indirect source of "coupling" is what we may describe

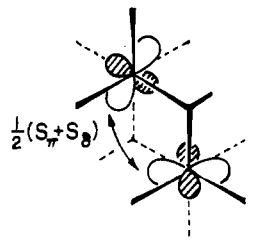

14

as through-bond coupling via d–p π interaction with the surrounding oxide ligands. We will not delve into the intricacies of such an analysis since our simple model does a rather effective job of describing the full calculation. In fact, since the high-symmetry lines of the Brillouin zone are regions of $\vec{k}$ space where degeneracies are indeed found in model bands, the extent to which the model and calculated results differ is perhaps exaggerated by examining the high-symmetry lines. General k points will show an even closer correspondence.

In the above discussion, we have gone to some lengths to establish a correspondence between our computed results for the Mo t_{2g} bands and a model in which xy, xz, and yz bands are considered independently. Since this correspondence greatly facilitates the analysis of the distorted systems to be treated below, we will often proceed using this qualitative tool. We should note that this model becomes inappropriate even for the related MoS_2 system (we are still discussing an octahedral layer, even though MoS_2 is itself trigonal prismatic). In the octahedral disulfide layer the average M–M contacts are considerably longer and the Mo–S d–p π interaction is greater because the electronegativity difference between Mo and S is smaller. As a result, the through-bond Mo–S–Mo coupling becomes an important influence on the form of t_{2g} dispersion curves.

For the case of a MoO_2 layer, the approximate independence of the xy, xz, and yz manifolds suggests a simple scheme for generating and examining potential distorted structures. Consider, for example, the distorted layer structure of $Na_{0.85}Mo_2O_4$ in which the metal atoms form zigzag double chains within the layers. This arrangement can be seen as one in which two of the subsystems (xz, yz) have been perturbed by a pairing distortion while the third (xy) has been left unaltered. The structural situation is indicated schematically in **15**, while the expected electronic structure scheme

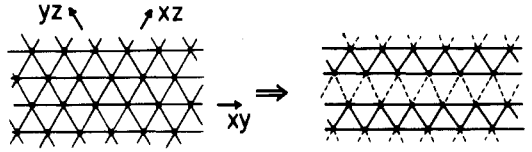

15

is given in **16**. The position of the Fermi level as a function of

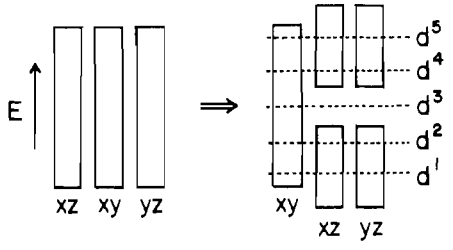

16

electron count is indicated as well. Thus, for $Na_{0.85}Mo_2O_4$ ($d^{2.43}$), one expects the lower (bonding) xz and yz bands will be essentially fully occupied and the xy band is available to take up electrons in excess of 2 per Mo atom.

The superposition of pairing distortions in the independent xy, xz, and yz systems can be used as a means of generating metal–metal-bonding networks within MoO_2 layers. One may be slightly more general and make use of the implications of pairing distortions to place restrictions on the kinds of metal–metal linkages a single center will participate in forming. A d^1 center will form just one short metal–metal bond. A d^2 center may form two such linkages, 60 or 120° from each other, but not 180°. A d^3 center will form three bonds, none of which will be 180° from another. The situation for d^2 and d^3 centers is illustrated in **17**.

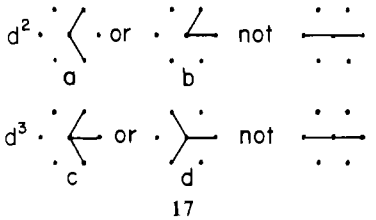

17

Prospective metal–metal-bonded networks may be built by merely linking together these units. It is not difficult to see that a superposition of pairing distortions can generate no other building blocks for metal–metal bonding within an MO_2 layer. However, the use of these building blocks may indeed generate a metal–metal-bonded network that is not describable as a superposition of pairing distortions. Thus, the metal–metal bonding in $Na_{0.85}Mo_2O_4$ may be described as the linking of the units in **17b**, while $LiVO_2$ has been proposed[13] as consisting of metal–metal-bonded triangles at low temperatures ($LiVO_2$ may be thought of as a VO_2 layer compound with intercalated Li); see **18**. The latter

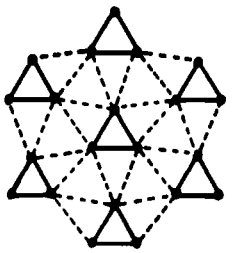

18

pattern is, of course, just another way of linking the units in **17b** and cannot be described as a superposition of pairing distortions. Though outside of our professed realm of the dioxides, $ReSe_2$[14,15] represents an example in which the units of **17c** are linked to form a very distorted system of connected clusters, as in **19**. Patterns built from more than one of the building blocks in **17** may also be easily constructed. A layer consisting of rhombuses as in **20** is built from **17b** and **17c** while **17c** and **17d** can be used to construct the pattern **21**.

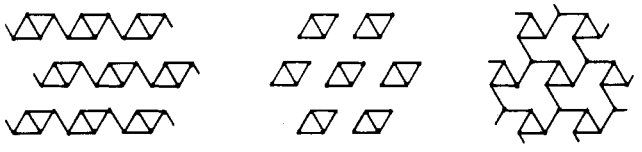

19 20 21

(13) (a) Bongers, P. F. *Chem. Weekbl.* **1967**, *63*, 353. Bongers, P. F., quoted by: Goodenough, J. B. "Magnetism and the Chemical Bond"; Interscience: New York, 1963; p 270. (b) Bongers, P. F. "Crystal Structure and Chemical Bonding in Inorganic Chemistry"; Rooymans, C. J. M., Rabenau, A., Eds.; North Holland: Amsterdam, 1975; pp 27–45.

(14) (a) Alcock, N. W.; Kjekshus, A. *Acta Chem. Scand.* **1965**, *19*, 79. (b) Marolikas, C.; Amelinckx, S. *Physica B+C (Amsterdam)* **1980**, *99B+C*, 31. (c) The system Cu_xVS_2 exhibits distortions derived from the basic building block in **17**: Nagard, N.; Collin, G.; Gorochov, O. *Mater. Res. Bull.* **1977**, *12*, 975; **1979**, *14*, 155.

(15) For a recent theoretical treatment of $ReSe_2$ see: Kertesz, M.; Hoffmann, R. *J. Am. Chem. Soc.* **1984**, *106*, 3453.

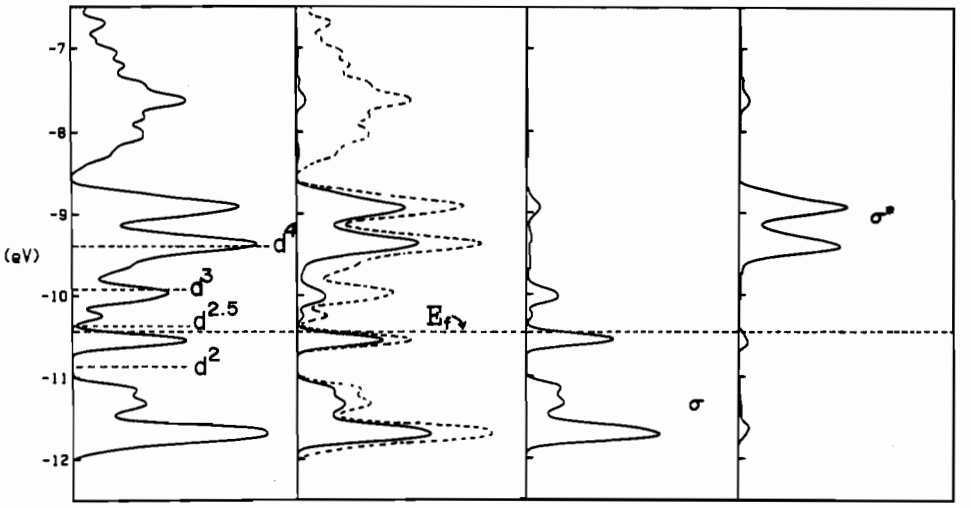

Figure 3. Density of states (DOS) diagrams for the MoO_2 layer with zigzag chains. The far left panel shows the total DOS; in the center left panel the d orbitals directed for σ interaction along the short Mo–Mo bonds are projected. The center right and far right panels show the "σ" and "σ^*" contributions for these bonds; see **22**.

It is clear that we have moved from a delocalized picture of bonding in considering an undistorted MO_2 octahedral layer to a localized picture for potential distorted variants in which we have gone so far as to associate each close metal–metal contact with a 2 center–2 electron (2c–2e) bond. This transition in our viewpoint had some justification insofar as an approximate correspondence was found to exist between the t_{2g} d bands of an undistorted MoO_2 layer and that of a model employing three independent (xy, xz, and yz) d bands. However, we have gone a step further and assumed that each subsystem behaves as one-dimensional in that half-filled bands are expected to result in pairing (Peierls) distortions.[16] This step is not well justified in that each metal t_{2g} orbital is coupled to all of its neighbors, not just those with which it forms σ interactions (see **12**). Notwithstanding these reservations, the scheme outlined above serves as a crude framework in which we may examine more detailed results. It is tempting to account for clustering in these systems by assigning each close metal–metal contact as a 2c–2e bond. The foregoing treatment makes explicit that which is neglected in yielding to this temptation.

Zigzag Chain Structures and Distorted Variants

To investigate the electronic structure of $Na_{0.85}Mo_2O_4$, we have performed calculations on a single distorted two-dimensional MoO_2 layer (as illustrated in **8**). All Mo–O contacts were set equal to 2.08 Å; short Mo–Mo distances were 2.53 Å, Mo–Mo distances parallel to the direction of propagation were 2.87 Å, and interchain Mo–Mo distances were 3.22 Å. This calculated geometry simply results from shifting every other string of Mo atoms in an ideal hexagonal MoO_2 layer (lattice constant 2.87 Å) by 0.4 Å to form the zigzag double chains of **8**. Our calculated geometry represents only a slight idealization of the MoO_2 layers as they are found in the observed structure. Although the Mo array is far from the ideal hexagonal arrangement, the oxygens so closely follow the metal atom distortion that the Mo–O distances fall within a range of 0.04 Å. In the left panel of Figure 3, we show the total density of states (DOS) that results from our calculation. Only the Mo d bands are given, the oxide s and p bands lying at lower energy. As can be seen from the figure, only the gross features that were found in the calculation of the ideal hexagonal layer survive in the distorted case. As before, there is a separation of the e_g and t_{2g} bands but the t_{2g} bands have suffered considerable perturbation upon distortion to form zigzag Mo chains. A gap has opened at the d^2 electron count, and some deep local minima are found throughout the −12.0 to −8.5 eV energy range. An interpretation of the DOS can be made by projecting appropriate orbital contributions as is done in the remaining panels of Figure 3. In the second panel we project the contribution from the d orbitals that are directed for σ overlap along the short bonds of the zigzag chain; i.e., the xz and yz orbitals we discussed in reference to **11**. In qualitative terms this distribution reflects what was anticipated in the scheme of **16**; there are large contributions at the top and bottom of the t_{2g} block with relatively little in the center of that energy range. The remaining Mo contribution to the DOS in this energy range comes almost entirely from xy, the remaining t_{2g} orbital. The remaining two panels of Figure 3 show the xz and yz orbitals projected in another way, as σ and σ^* combinations illustrated in **22**. It can be seen that for the electron count

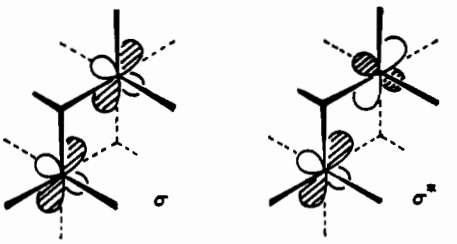

22

appropriate for $Na_{0.85}Mo_2O_4$, $d^{2.43}$, the σ combination is virtually full while σ^* remains empty.

The scheme given in **16** is in reasonable accord with the information conveyed in Figure 3. However, certain details such as the gap found at d^2 simply cannot emerge from the kind of analysis given. This kind of result can be understood only after a reasonably detailed examination of the energy bands of the system in question, which we will not give.

In order to investigate the intrinsic differences between the metal–metal bonding in zigzag chains embedded in layers and those embedded in a hollandite framework, we performed calculations to examine the latter system. The geometrical parameters chosen for this calculation were quite similar to those described above for the layer calculation; all bond lengths were kept as before, and the trigonal oxides linking the double chains were constrained to lie in the plane of their surrounding Mo neighbors. The structure is simply that which is depicted in **9**; metal–metal contacts within the zigzag chains were the same in both systems. We will not bother to present any pictorial data that describe the results of this calculation for the simple reason that the DOS in the d-band region does not appreciably differ from that obtained for the layer system. Comparison of the more detailed dispersion curves for the appropriate lines in the Brillouin zones for the two cases also reveals no striking differences in the partially occupied d bands. It might have been thought that because the interchain metal–metal contacts are smaller in the layer system than in the

(16) Peierls, R. "Quantum Theory of Solids" Clarendon: Oxford, England, 1955; p 108.

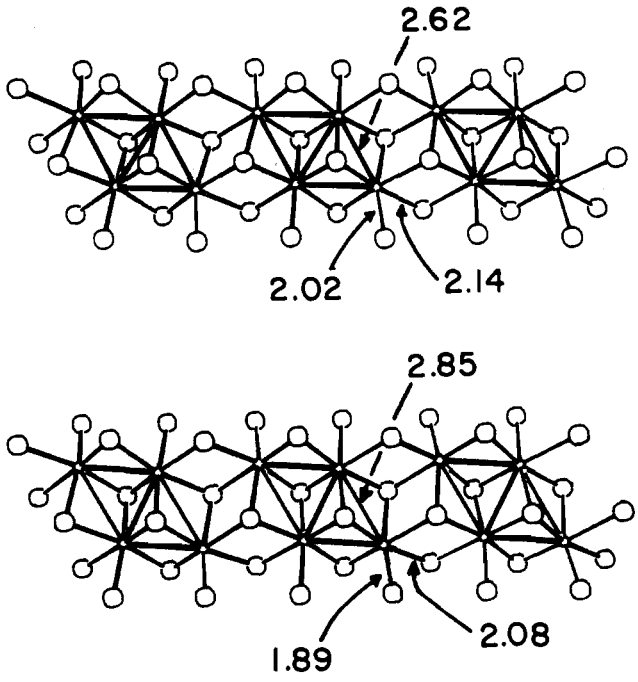

Figure 4. Structural details for the chains in $Ba_{1.14}Mo_8O_{16}$.

hollandite analogue (3.22 vs. 3.86 Å), the latter system would be expected to display a more "one-dimensional" behavior in the dispersion of the metal bands transverse to the chain direction. However, the bulk of such dispersion is due to the coupling provided by the intervening oxides for metal–metal separations of these magnitudes. We conclude that the principal differences between zigzag Mo chains embedded in these alternative oxide matrices is a result of the fact that in the hollandite structure type the oxides linking the double chains are trigonal planar rather than pyramidal. In support of this conclusion are the Mo–O overlap population differences involving pyramidal vs. planar oxides. For the latter bonds the average overlap populations[17] are calculated to be 0.33 but for the former only 0.27. We have been unable to find any other compelling reasons to expect a greater tendency for clustering in the hollandite analogue as opposed to the layer structure from consideration of the two idealized structures.

A better understanding of the occurrence of clustering in the pseudohollandite $Ba_{1.14}Mo_8O_{16}$ is gleaned from studying the details of the observed structure and the results of a calculation on the MoO_2 framework found in that compound. In Figure 4 we show the two types of chains reported for this compound. At the top is the chain containing regular clusters, and at the bottom is that which contains distorted clusters. In each chain 12 symmetry-inequivalent Mo–O bonds can be identified (a point of inversion lies at the center of each cluster and hence reduces the number of linkages from 24). A comparison of corresponding bond lengths between chains shows that the lengths of only two Mo–O bonds differ by greater than 0.02 Å from one chain to the other. These bonds are indicated in the figure as is the Mo–Mo bond that becomes lengthened in the distorted cluster. A single bridging trigonal-planar oxide is implicated as the villain of the piece, and this atom is appropriately shady in Figure 5. Because each of the trigonal-planar oxides serve to stitch together the distorted and undistorted chains, a motion of just the shaded oxides toward the distorted clusters is sufficient to generate the only significant difference between the distorted and undistorted chains insofar as Mo–O bonding is concerned. Further, this examination reveals the synergy between asymmetries in Mo–O bonding and Mo–Mo bonding in distorted clusters of the hollandite analogue $Ba_{1.14}Mo_8O_{16}$. The role of electron count in determining this structural fine tuning is underscored by the recent synthesis of the isoelectronic $K_2Mo_8O_{16}$,[10] in which the metal–metal and metal–oxygen contacts and their interrelationship are quite similar to what we have described above.

Detailed band calculations provide rather striking confirmation for most of the suppositions put forward by McCarley and Torardi in their original report of the synthesis of $Ba_{1.14}Mo_8O_{16}$.[3] In that report, the authors assigned a formal d-electron count of 10 to the undistorted clusters in this compound and had supposed the

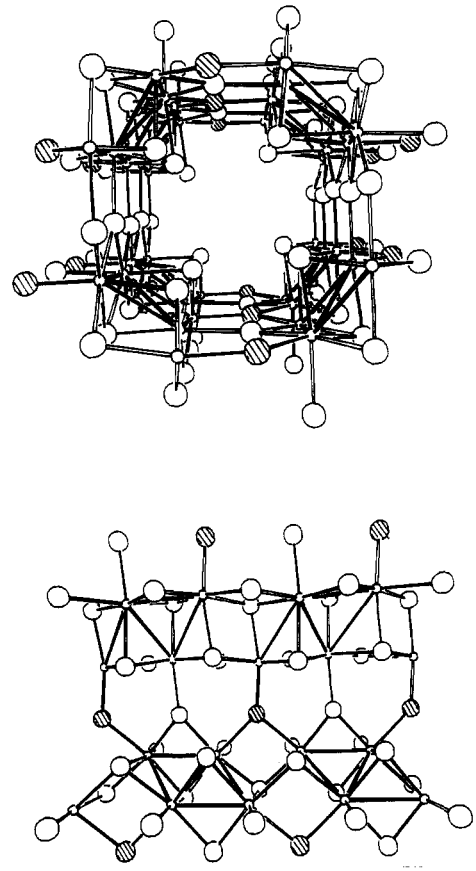

Figure 5. View of the MoO_2 hollandite network in $Ba_{1.14}Mo_8O_{16}$. Shaded oxides are those that "move" in the "formation" of distorted clusters. In the top illustration the position of these atoms is shown within the hollandite MoO_2 framework. The bottom illustration shows how these atoms are positioned relative to the clusters within the double chains.

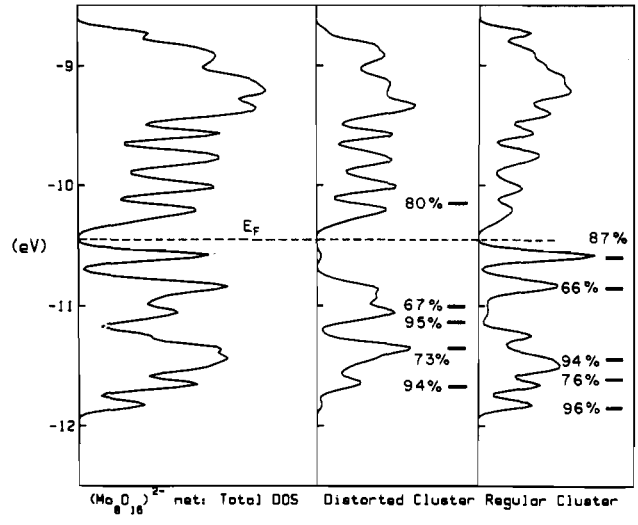

Figure 6. Total DOS in the "t_{2g}" band range for $Ba_{1.14}Mo_8O_{16}$. In the center and right panels, respectively, we show the Mo contributions of the distorted and regular clusters. The levels indicated within these panels are for the $\Gamma(k = 0)$ point in the Brillouin zone; the percentages indicate the extent of localization of these levels on the corresponding clusters.

(17) Mulliken, R. S. *J. Chem. Phys.* **1955**, *23*, 1833, 2343.

distorted cluster to be an 8-electron system. In Figure 6 we show the DOS calculated for this compound in the energy range of the "t_{2g}" Mo d bands. The contributions of the Mo atoms of the undistorted and regular clusters are respectively given in the middle and right panels of the figure. Also included in these panels are the lowest 10 energy levels for the $\Gamma(\bar{k} = 0)$ point in the Brillouin zone. The lines signifying these levels have been placed into the middle or right panels according to whether they are primarily localized on the chains of the distorted or regular cluster, respectively. The percentage contribution made to each crystal orbital by the clusters is indicated and was computed from a Mulliken population analysis where the contributions made by the bridging trigonal-planar atoms were evenly divided between each chain. The close correspondence between the positions of the Γ-point levels and the peaks of the full DOS calculation, along with the percentages given, indicates that considerable localization has been induced by the formation of the distorted chains. It is clear that if no such distortion had occurred, each of these levels would be equally delocalized over all the clusters. It is equally notable that four Γ-point levels associated with the distorted cluster and five Γ-point levels of the regular cluster fall below the Fermi level; this is nicely in consonance with 8- and 10-electron counting schemes originally proposed for these clusters. Indeed, if one uses the results of the full calculation and integrates over the nine occupied formal "d bands", 9.84 and 8.16 electrons can be assigned to the chains of the regular and distorted clusters, respectively. Additionally, the total charges on each cluster are calculated to be 1.71– and 0.29–, respectively. This unusually close correspondence between *computed* charges and the expected *formal* charges is another strong indication of the extent to which the formation of distorted clusters induces localization.

At this point we should note the close similarity between the levels we have indicated for $\bar{k} = 0$ in Figure 6 and the MO level diagrams obtained for calculations on discrete clusters by Cotton and Fang.[18] Basing their discussion on the results of Fenske–Hall calculations, these workers nicely show how the 8-electron cluster can be explained as subject to a second-order Jahn–Teller distortion. We have not presented our results so as to highlight this feature, but insofar as the driving force is derived from changes in metal–metal bonding this is in accord with our discussion.

The more electron-rich $RuO_2^{0.33-}$ hollandite system found in $BaRu_6O_{12}$ is an example in which the relative importance of metal–metal bonding is overshadowed by metal–oxide π bonding. On the basis of the Ru–Ru distances found in this material (>2.9 Å), one might expect direct through-space interaction to be rather weak. Additionally, each potential metal–metal bond in the structure is doubly bridged by oxides (i.e., the RuO_6 octahedra share edges). The effect of intervening bridging groups on metal–metal bonding has been noted in previous work.[19] Generally, when metal–metal distances are fairly long, the conventional ordering of metal–metal-bonding and metal–metal-antibonding levels may be inverted through interaction with orbitals of the bridging atoms. As a result, when metal-based levels are even partially occupied, they are as likely to be antibonding as bonding.

The above statements are amplified when we examine the results of calculations on a RuO_2 net in which all Ru–Ru distances were set equal to 3.0 Å. The gross features of the DOS for this system are similar to our results for the MoO_2 hollandite system (i.e., the oxide p bands and the Ru t_{2g} bands are readily identifiable). To make our point concerning the importance of Ru–O π bonding, we show that portion of the DOS attributable to the trigonal-planar oxides in Figure 7. The dashed line gives the total contribution to the DOS made by these atoms; the full line gives the contribution of just the p π orbitals on these atoms. Note that the Fermi level lies high up in the t_{2g} bands (appropriate for a $d^{4.33}$ system) and is just below a large peak in the curve for the p π orbital. The

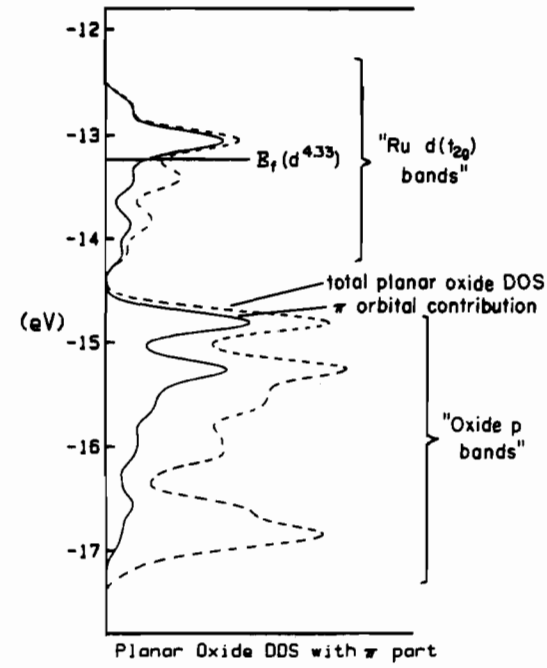

Figure 7. Contribution of trigonal-planar linking atoms in a RuO_2 hollandite. The solid line is the contribution made by the p orbital normal to the plane of the oxide and its Ru neighbors.

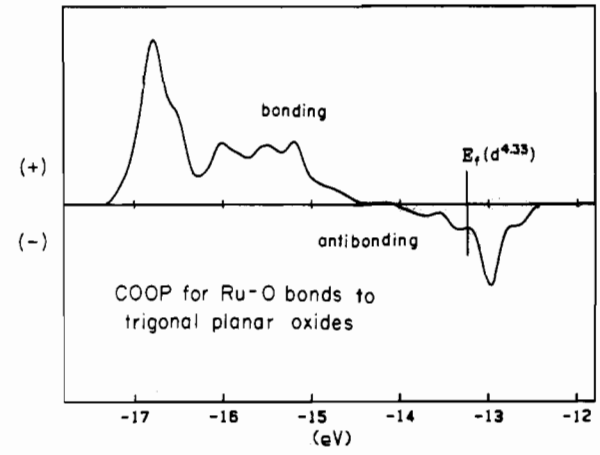

Figure 8. Crystal orbital overlap population (COOP) curve for the Ru–O bonds involving trigonal-planar oxides in the RuO_2 hollandite. This curve represents the average over the two types of bonds actually present in the structure. Note the position of the Fermi level in this figure and Figure 7.

meaning of this peak can be ascertained by examining the crystal orbital overlap population (COOP)[19b] curves for the bonds between Ru and the trigonal-planar oxides. These curves enable one to determine at a glance whether levels in a given energy range are bonding (or antibonding) according to whether the curves take on positive (or negative) values in the energy range of interest. As shown in Figure 8, the COOP curves for these Ru–O bonds turn strongly negative just above the Fermi level. The conclusion we may draw is that this system manages to avoid the filling of Ru–O π^* levels—a result that is difficult to demonstrate by examining metal-based d contributions to the DOS directly because of geometrical difficulties in the calculations which are involved. We may further note that the average Ru–O bond length involving trigonal-planar oxides is observed to be 0.09 Å shorter than the average Ru–O distance involving pyramidal oxides, in line with the trend we find for the corresponding overlap populations (0.40 vs. 0.35—all Ru–O distances were set equal in the calculation at the observed average value of 2.0 Å). As for Ru–Ru bonding, the Ru–Ru overlap populations were slightly negative and hence no appreciable metal–metal bonding was indicated.

(18) Cotton, F. A.; Fang, A. *J. Am. Chem. Soc.* **1982**, *104*, 113.
(19) (a) Shaik, S.; Hoffmann, R.; Fisel, C. R.; Summerville, R. H. *J. Am. Chem. Soc.* **1980**, *102*, 4555. (b) Hughbanks, T.; Hoffmann, R. *J. Am. Chem. Soc.* **1983**, *105*, 3528. (c) Burdett, J. K.; Hughbanks, T. *J. Am. Chem. Soc.* **1984**, *106*, 3101.

Utilizing the scheme of Bart and Ragaini,[20] McCarley et al. have demonstrated a remarkable correlation between Mo–O bond length averages and formal cluster electron counts for a variety of newly synthesized compounds closely analogous to that considered here. Examination of the computed charges is in this case in line with the trend expected from a consideration of the observed Mo–O bond length averages about each of the four unique Mo atoms in the $Ba_{1.14}Mo_8O_{16}$ structure. In **23** we show the computed

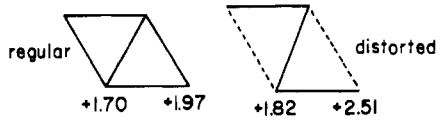

23

charges and parenthetically include the average Mo–O bond length about the corresponding Mo. The major difference between the distorted and regular clusters is at the Mo atoms occupying the vertices of the acute angles of the 4-metal clusters. It should be noted that the averaging of the Mo–O bond lengths tends to give the impression that the small difference shown may not be significant, but as we discussed above, the origin of this difference is traceable to a difference in the position of a *single* O atom. Whether there exists a systematic correlation between bond-valence approaches and calculations such as ours is a matter we will leave for future investigation.

A question that we must have unanswered, at least in the strongest sense, is why in the pseudohollandite $Ba_{1.14}Mo_8O_{16}$ the zigzag metal–metal-bonded chains distort to form clusters while in $Na_{0.85}Mo_2O_4$ such chains survive undistorted. The low symmetry, relatively large unit cell, and the large variation among the Mo–O bond lengths of the $Ba_{1.14}Mo_8O_{16}$ structure preclude the calculation of any kind of reasonable surface connecting the undistorted pseudohollandite structure with the structure observed. The deficiencies of our calculations in getting correct bond lengths would cast strong doubts over the results of such an effort in any case. Given that the pseudohollandite structure does exhibit distorted clusters, it seems likely that a more electron-rich pseudohollandite structure with 10 e/Mo_4 unit would form chains with regular rhombic clusters rather than with extended zigzag chains. As we have said above, however, it is the ability of trigonal-planar linking oxides to participate as π donors that appears to be involved here. With this in mind it is interesting to consider what effect Li insertion might have on a pseudohollandite system. Would Li^+ insert into rutile-like small interstices in the hollandite structure? If the host structure is rugged enough to withstand the physical strain such distortion would place on a crystal, might a process as depicted in **24** occur?[21] (Note the

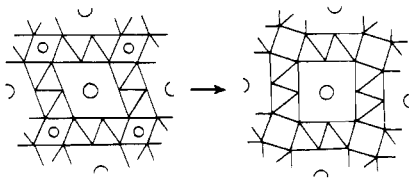

24

analogy with **7**.) Finally, since this process would pyramidalize the oxides involved in π bonding with the metals, the transition metals may prefer to form undistorted chains rather than clusters.

Are there circumstances under which we would expect the MoO_2 layer to exhibit clustering as opposed to zigzag chain formation? In Figure 9 we show the energetics, as a function of the d-electron count, of distorting an ideal hexagonal layer to the zigzag chain structure **8** and to a structure consisting of rhombuses

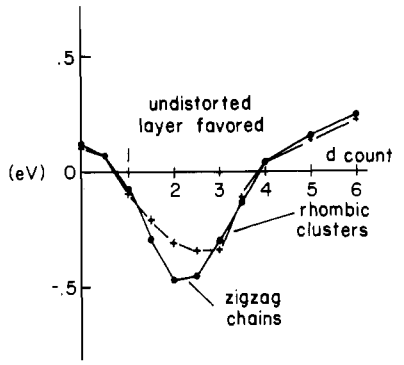

Figure 9. Relative energy curves for the MoO_2 layer with zigzag chains (as in $Na_{0.85}Mo_2O_4$) and a layer with embedded Mo_4 rhombic clusters vs. a hexagonal MoO_2 layer as a function of the metal d-electron concentration. Where the curves are below (above) the base line, the distorted structures are calculated to be more (less) stable.

embedded in a hexagonal layer (as shown in **20**). Geometrical constraints on the latter structure were as in other layer calculations; Mo–O bond lengths were kept constant and therefore "followed" the distortion considered for the metal atoms. There is not much in these curves to distinguish these two cases from each other, but both curves indicate the generic instability of the ideal MoO_2 layer, especially for d counts from 1.5 to 3. The zigzag chain enjoys the greatest relative stability for $d^{2.0}$–$d^{2.5}$: the difference between the chain structure and the clusters appropriate for $Na_{0.85}Mo_2O_4$ is approximately 2.3 kcal/Mo atom (or about 9 kcal/cluster). The energetics do not reflect the precise trends expected on the basis of the crude model discussed earlier since the structure containing clusters would have been predicted to hold sway for a system with 10 e/rhombus. If such clustering is to be expected at all we find it to be most likely for a d^3 system.

We have investigated various alternative clustering patterns in order to see whether some sort of "map" of structure type vs. electron count could be constructed. Although the results show some similarities to the plots of Figure 9, too many structural competitors lie in too narrow an energy range to draw any strong conclusions about their relative stabilities. This result is perhaps to be expected: we know, for example, that characteristic electron counts for trinuclear and tetranuclear clusters overlap. Triangular clusters typically possess 6–8 metal electrons,[22-24] while the rhombic clusters hold from 8 to 10 metal electrons. At least for now, the results of synthetic efforts in this area will hold as much surprise as ever!

The Trigonal-Prismatic Alternative

While not the principal focus of this work, when dealing with MX_2 systems with d^2 transition metals, the possibility that trigonal-prismatic layer compounds will be found must be considered. Indeed, $LiNbO_2$ is found to adopt a filled MoS_2 structure in which Li atoms occupy octahedral holes between trigonal-prismatic NbO_2 layers.[25] That a d^2 ion will assume trigonal-prismatic coordination has longstanding precedent in solid state (e.g., MoS_2) and molecular systems.[1]

Calculations on a single (NbO_2^-) layer were performed to investigate whether the observed octahedral vs. trigonal-prismatic preferences would emerge in our treatment. Since our results

(20) (a) Bart, J. C. J.; Ragaini, V. *Inorg. Chim. Acta* **1979**, *36*, 261. (b) For a general review of bond-valence methods see: Brown, I. D. "Structure and Bonding in Crystals"; O'Keeffe, M., Navrotsky, A., Eds.; Academic Press: New York, 1981; Chapter 14.

(21) See the discussion of $CaFe_2O_4$ in: Plug, C. M. *J. Solid State Chem.* **1982**, *41*, 23.

(22) Six-electron clusters in oxides: (a) McCarroll, W. H.; Katz, L.; Ward, J. *J. Am. Chem. Soc.* **1957**, *79*, 5410. (b) McCarroll, W. H. *Inorg. Chem.* **1977**, *16*, 3351. (c) For a discussion of six-electron clusters see: Muller, A.; Jostes, R.; Cotton, F. A. *Angew. Chem., Int. Ed. Engl.* **1980**, *19*, 875 and references therein.

(23) Seven-electron triangular clusters: (a) von Schnering, H. G.; Wohrle, H.; Schafer, H. *Naturwissenshaften* **1961**, *48*, 159. (b) A recently synthesized oxide is $ScZnMo_3O_8$: Torardi, C. C.; McCarley, R. E. *Inorg. Chem.* **1985**, *24*, 476.

(24) Eight-electron triangular clusters: (a) Bino, A.; Cotton, F. A.; Dori, Z. *Inorg. Chim. Acta* **1979**, *33*, L133. (b) $Zn_3Mo_3O_8$ was recently synthesized by Torardi and McCarley; see ref 22b.

(25) (a) Meyer, G.; Hoppe, R. *Angew. Chem.* **1974**, *86*, 819; *Angew. Chem., Int. Ed. Engl.* **1974**, *13*, 744. (b) $NaNbO_2$ is isostructural: Meyer, G.; Hoppe, R. *Z. Anorg. Allg. Chem.* **1976**, *424*, 128.

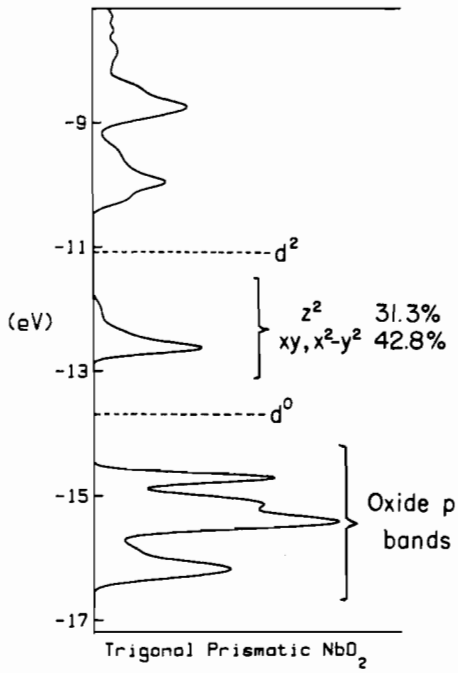

Figure 10. Total DOS for a trigonal-prismatic NbO_2 layer. The Fermi level for a d^0 and d^2 count is indicated.

closely parallel earlier theoretical treatments of analogous chalcogenides, we will be brief in our discussion. Figure 10 shows the DOS calculated for a trigonal-prismatic layer in which the structural parameters are as found in $LiNbO_2$. The Nb–O distance was taken to be 2.116 Å and the Nb–Nb distance was 2.90 Å. This implies that the angle from a line through the center of a triangular prism face (the z axis) to the lines of the Nb–O bonds is 52.4°, near to the value of 54.7° obtained by a 60° twist of one of the faces of an octahedron. For a trigonal-prismatic molecule we would expect that the crystal field would split the d levels into a pattern with $z^2 < x^2 - y^2, xy < xz, yz$. This level ordering persists to a large extent in the DOS of the trigonal-prismatic layer. However, as indicated in the figure, there is considerable mixing of the xy, $x^2 - y^2$ set into the lower lying "z^2" band. A similar result was obtained by Mattheiss in an augmented plane wave study of MoS_2 some time ago.[26] It seems likely that a scheme for the metal–metal bonding involving 3c–2e bonds as proposed by Nguyen et al.[27] for analogous sulfide systems containing embedded trigonal-prismatic layers could be appropriate for this system as well.

A comparison with an octahedral $(NbO_2)^-$ layer with the same lattice constant and Nb–O distance shows the trigonal-prismatic layer structure to be favored, but only for a d^2-electron count. A curve showing the relative energies of these two alternatives as a function of electron count is shown in Figure 11; where the curve is below the base line, the trigonal-prismatic structure is calculated to be more stable. Clearly, the stabilization of a single metal–metal-bonding band is responsible for enhanced stability of the trigonal-prismatic layer structure at the d^2 count. The relative stability of the octahedral layer at the d^0 count appears to be due to greater interlayer oxide–oxide repulsions in the trigonal-prismatic structure where such pairs of atoms are only 2.59 Å apart. This repulsion is manifested in the calculation by significantly negative overlap populations between these pairs of atoms. Above the d^2 count the relative energy of the octahedral layer is enhanced by the fact that, when octahedrally coordinated, the metals possess three d orbitals without any Nb–O σ-antibonding character but, when the metal is trigonal prismatic, only the z^2 orbital is σ nonbonding. The narrow range of stability for the trigonal-prismatic layer is notable when compared with the broader ranges

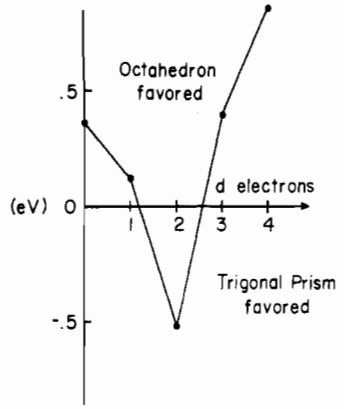

Figure 11. Relative energy of a trigonal-prismatic vs. octahedral NbO_2 layer as a function of d-electron concentration. The curve is to be interpreted in the same way as Figure 9.

Table I. Parameters for EH Calculations

atom (ref)	orbital	H_{ii}, eV	ζ_1^b	ζ_2^b	C_1^a	C_2^a
Nb (35)	5s	−10.10	1.89			
	5p	−6.86	1.85			
	4d	−12.10	4.08	1.64	0.6401	0.5516
Mo (34)	5s	−8.77	1.96			
	5p	−5.60	1.90			
	4d	−11.06	4.54	1.90	0.5899	0.5899
Ru	5s	−10.79	2.08			
	5p	−5.74	2.04			
	4d	−14.62	5.38	2.30	0.5573	0.6642
O	2s	−32.30	2.275			
	2p	−14.80	2.275			

[a] Coefficients used in the double-ζ expansion. [b] Slater-type orbital exponents.

of relative stability for structures based upon octahedral metals. Clearly, attempts to make compounds with trigonal-prismatic transition metals that are not d^2 (or perhaps d^1) are most likely to succeed if they are performed at low enough temperatures so that kinetic barriers separating trigonal-prismatic and octahedral structures cannot be surmounted.[6-8] Techniques where the integrity of the host matrix is preserved may be best for preparing compounds in which the transition metals are trigonal prismatic and have configurations other than d^2 or d^1.

We should note that the $LiNbO_2$ compound referred to above was reported to exhibit temperature-independent paramagnetism with a dependence on magnetic field strength and was therefore presumed to be antiferromagnetic.[24a] This is obviously at odds with the electronic structure depicted in Figure 10, where we predict a diamagnetic semiconductor with a band gap of approximately 1.4 eV. The semiconducting behavior of other d^2 trigonal-prismatic compounds such as MoS_2 makes the claimed magnetic behavior surprising. If indeed this compound is an antiferromagnet, the structure is certainly unexpected: the stability conferred upon a trigonal-prismatic structure for a d^2 count would be lost in such a "high-spin" analogue. We believe the reported magnetic properties of this system are the result of impurities and/or nonstoichiometry.

Finally, we have briefly considered whether one should expect a trigonal-prismatic oxide layer system to be susceptible to distortions driven by the formation of zigzag chains. In contrast to the octahedral d^2 case, no such tendency to distort was found from our calculations on a $(MnO_2)^-$ trigonal-prismatic layer deformed to give zigzag chains like those found in $Na_{0.45}Mo_2O_4$. Steric constraints, again manifested as oxide–oxide repulsions across the layer, restrain motion of the Nb atoms away from positions in an ideal hexagonal net (Nb–O distances were assumed to remain constant in the distorted structure). Furthermore, because the "z^2 band" is split off from the rest of the d block in the trigonal-prismatic case, when this band is fully occupied, the trigonal-prismatic layer behaves more as a closed-shell system. Thus, the energy difference between the ideal and distorted trigonal-

(26) Mattheiss, C. F. *Phys. Rev. B: Solid State* **1973**, *B8*, 3719.
(27) Nguyen, T.-H.; Franzen, H.; Harmon, B. N. *J. Chem. Phys.* **1980**, *73*, 425.

prismatic layer is 0.35 eV/Nb atom for a d^0 count and increases slightly to 0.43 eV for a d^2 count. On the other hand, for a d^1 count we found this energy difference shrinks to 0.1 eV with the undistorted structure still favored. The shrinking of this energy difference is not unexpected in light of the known structural and electronic instabilities of analogous d^1 dichalcogenides.[28]

Acknowledgment. We thank the donors of the Petroleum Research Fund, administered by the American Chemical Society, for their partial support of this research and the National Science Foundation via NSF Grant DMR 8019741.

Appendix

All calculations were of the extended Hückel type[30] with the parameters and exponents of Table I. The weighted Wolfsberg-Helmholz formula was used.[31,32] H_{ii} values for Ru were obtained by charge iteration[33] on the actual RuO_2 net possessing a charge of $^1/_2$-/RuO_2 unit. Sources of other atomic parameters are indicated in the table. The geometrical particulars of the systems studied are described above except coordinates for $Ba_{1.14}Mo_8O_{16}$ which were graciously supplied by Professor R. McCarley. We extend thanks to Dr. Charles Torardi for providing results on $BaRu_6O_{12}$ and $K_2Mo_8O_{16}$ prior to publication.

In all calculations in crystals, matrix elements were computed between atoms separated by less than 5.94 Å. $\vec{k}$-Point meshes employed in crystalline calculations were as follows: for the two-dimensional ideal octahedral MoO_2 and NbO_2 slabs and the trigonal-prismatic NbO_2 slab, 105 $\vec{k}$ points (2-D hexagonal lattice); for the MoO_2 sheets of $Na_{0.45}Mo_2O_4$ and the analogous zigzag distorted trigonal-prismatic NbO_2 layer, 100 $\vec{k}$ points (2-D rectangular lattice); for the idealized MoO_2 and RuO_2 hollandite analogues, 40 $\vec{k}$ points (body-centered tetragonal); for the actual MoO_2 net of $Ba_{1.14}Mo_8O_{16}$, 32 $\vec{k}$ points (triclinic). Discussion of the bonding of $Na_{0.45}Mo_2O_4$ closely parallels the methodology outlined in ref 29.

Registry No. MoO_2, 18868-43-4; RuO_2, 12036-10-1; $BaMo_8O_{16}$, 52934-88-0; NbO_2, 12034-59-2.

(28) See, for example: Hulliger, F. *Struct. Bonding (Berlin)* **1968**, *4*, 83. Levy, F., Ed. "Crystallography and Crystal Chemistry of Materials with Layered Structures"; Reidel: Boston, 1976.
(29) Hughbanks, T.; Hoffmann, R. *J. Am. Chem. Soc.* **1983**, *105*, 1150.
(30) Hoffmann, R. *J. Chem. Phys.* **1963**, *39*, 1397.
(31) Ammeter, J. H.; Burgi, H. B.; Thibeault, J.; Hoffmann, R. *J. Am. Chem. Soc.* **1978**, *100*, 3686.
(32) Summerville, R. H.; Hoffmann, R. *J. Am. Chem. Soc.* **1976**, *98*, 7240.
(33) Baranovskii, V. I.; Nikolskii, A. B. *Theor. Eksp. Khim.* **1967**, *3*, 527.
(34) Kubacek, P.; Hoffmann, R.; Havlas, Z. *Organometallics* **1982**, *1*, 180.
(35) Whangbo, M.-H.; Hoffmann, R. *J. Am. Chem. Soc.* **1978**, *100*, 6093.

Contribution from the Department of Chemistry and Laboratory for Molecular Structure and Bonding, Texas A&M University, College Station, Texas 77843

Molecular Mechanics of Low Bond Order Interactions in Tetrakis(carboxylato)dimetal Systems

JAN C. A. BOEYENS,*† F. ALBERT COTTON,* and SCOTT HAN

Received June 6, 1984

The influence of steric factors on the lengths of metal-metal bonds of various orders has been examined by using molecular mechanics calculations. The variation in bond distances exhibited by dirhodium(II) systems, $Rh_2(XYCR)_4L_2$ (X, Y = S, O), is shown to be well explained by steric forces. Bond lengths are predicted for some as yet unknown but makable molecules. The short Rh-Rh distance in $Rh_2(O_2CCH_3)_4(H_2O)_2$ is shown to result from a compressive effect by the bridging acetate groups as proposed by Norman and Kolari. Calculations on Pd_2^{4+}, Cu_2^{4+}, and Cd_2^{4+} complexes, where it is generally accepted that no significant metal-metal bonds exist, account well for the observed metal-metal distances. Finally, a general concept for correlating bond orders, bond lengths, and bond energies in dimetal systems with a range of bond orders (0-4) is presented and discussed.

Introduction

The variation of bond length with order for bonds between metal atoms is relatively complicated compared with the behavior of simple covalent bonds.[1] This is due to the more flexible electronic configuration of transition metals and aggravated by steric interactions that occur in the fairly complicated structures often employed to stabilize metal-metal bonds of different order. Rationalization of the observed trends would be greatly facilitated by separating steric from electronic factors, and this can be achieved by the method of molecular mechanics. This model[2] treats a molecule as a set of pairwise, mechanically interacting atoms and yields an equilibrium arrangement corresponding to a minimum in the steric energy as a function of all interactions and atomic coordinates.

Our treatment begins with the (purely hypothetical) configuration that would exist if each bond length and each bond angle were individually to have the value determined only by its own intrinsic electronic properties. We then seek the *arrangement of minimum strain*, which is the one that is obtained by minimum distortion of the idealized arrangement, consistent with electronic considerations, that can be obtained without disturbance of any electronic factor. For a bond distortion this would, for instance, correspond to displacement along the characteristic potential energy Morse curve for a bond of appropriate order.[3]

The electronic factors are incorporated into the definition of the force field, which includes force constants, bond orders, and van der Waals interactions between atoms separated by a sequence of more than three chemical bonds. The force field having been adopted, all interactions are then calculated exactly. Any discrepancies between calculated and observed structure parameters must be ascribed either to an inappropriate force field or to experimental errors in the observed structure. All steric factors have now been taken into account.

Experimental Section

There is some concensus on the definition of a force field for organic molecules,[4] and although the situation is more fluid for inorganic systems, sufficient guidelines exist[5,6] to ensure that most force fields yield results that are in qualitative agreement.[7] The force field adopted for the

† On leave from the Department of Chemistry, University of the Witwatersrand, Johannesburg, South Africa.

(1) Cotton, F. A. *Chem. Soc. Rev.* **1983**, *12*, 35.
(2) White, D. N. J. *Mol. Struct. Diffr. Methods* **1978**, *6*, 38.
(3) Boeyens, J. C. A.; Ledwidge, D. J. *Inorg. Chem.* **1983**, *22*, 3587.
(4) Allinger, N. L. *J. Am. Chem. Soc.* **1977**, *99*, 8127.
(5) Scott, R. A.; Scheraga, H. A. *J. Chem. Phys.* **1965**, *42*, 2209.
(6) Brant, D. A.; Flory, P. J. *J. Am. Chem. Soc.* **1965**, *87*, 2788.
(7) Boeyens, J. C. A.; Levendis, D. C. *J. Chem. Phys.* **1984**, *80*, 2681.

0020-1669/85/1324-1750$01.50/0